Materials Today Communications 24 (2020) 101111

Contents lists available at ScienceDirect

Materials Today Communications

journal homepage: www.elsevier.com/locate/mtcomm

Nitrogen-Doped microporous carbons derived from azobenzene and nitrile-functionalized polybenzoxazines for CO_2 uptake

Mohamed Gamal Mohamed[a,b], Mei-Yin Tsai[a], Wei-Chen Su[a], Ahmed F.M. EL-Mahdy[a,b], Chih-Feng Wang[c], Chih-Feng Huang[d], Lizong Dai[e], Tao Chen[f], Shiao-Wei Kuo[a,g,*]

[a] Department of Materials and Optoelectronic Science, Center of Crystal Research, National Sun Yat-Sen University, Kaohsiung, Taiwan
[b] Chemistry Department, Faculty of Science, Assiut University, Assiut 71516, Egypt
[c] Advanced Membrane Materials Research Center, Graduate Institute of Applied Science and Technology, National Taiwan University of Science and Technology, Taipei, 10607, Taiwan
[d] Department of Chemical Engineering, National Chung Hsing University, 145 Xingda Road, Taichung 402-27, Taiwan
[e] Department of Material Science and Engineering, Fujian Provincial Key Laboratory of Fire Retardant Materials, College of Materials, Xiamen University, Xiamen, Fujian 361005, China
[f] Ningbo Institute of Material Technology and Engineering, Chinese Academy of Science, Zhongguan West Road 1219, 315201 Ningbo, China
[g] Department of Medicinal and Applied Chemistry, Kaohsiung Medical University, Kaohsiung 807, Taiwan

ARTICLE INFO

Keywords:
Polybenzoxazine
Nitrogen-Doped microporous carbons
CO_2capture

ABSTRACT

In this study we synthesized two nitrogen-doped microporous carbons (NMCs) from the benzoxazine monomers BZAPh and BZACN through a process of curing polymerization, calcination, and KOH activation. We prepared the benzoxazine monomers BZAPh and BZACN in high yield and purity through Mannich reactions of 1,3,5-tris (4-aminophenoxy)benzene (TriPh-3NH_2), paraformaldehyde, and 4-phenylazophenol and 4-[(4-hydroxyphenyl) diazenyl] benzonitrile, respectively, in 1,4-dioxane. We employed differential scanning calorimetry (DSC), temperature-dependent Fourier transform infrared (FTIR) spectroscopy, and thermogravimetric analysis (TGA) to characterize the ring opening polymerization and thermal stability of the uncured monomers BZAPh and BZACN and the products of their thermal treatment at various temperatures. In addition, we used TGA, wide-angle X-ray diffraction (XRD), Raman and X-ray photoelectron spectroscopies (XPS), transmission electron microscopy (TEM), and Brunauer–Emmett–Teller (BET) analyses to examine the surface areas, porous structures, surface morphologies, chemical compositions, and thermal stabilities of these two highly N-doped NMCs. The NMC derived from the BZACN monomer, possessing both azobenzene and nitrile functionalities, exhibited superior thermal properties and CO_2 capture ability because it contained a high crosslinking density of the triazine functional groups after thermal curing.

1. Introduction

Porous carbon materials displaying chemical resistance, high surface areas, large pores, large pore volumes, biocompatibility, and excellent electrical conductivity have much attracted attention in both industrial and academic fields [1–6]. Because of their unique characteristics, these porous carbon materials have many potential applications in, for example, drug delivery, sensor technology, gene therapy, catalysis, SO_2 adsorption, CO_2 uptake, Li–S batteries, and electrochemical energy storage [7–11]. Furthermore, the preparation of nitrogen (N)-doped porous carbon materials has become interesting because of their ability to uptake CO_2; the incorporation of the N heteroatoms can improve the chemical properties and polarity of the carbon material and, thereby, enhance its interactions with molecules of CO_2 [12–16]. The literature describes many methods for the preparation of N-doped porous carbon materials, including chemical vapor deposition; solvothermal, segregation, and condensation reactions; thermal decomposition; polymer precursor approaches; reactions of melamine with porous carbon; and carbonization and KOH-activation processes of N-containing materials [17–20].

Polybenzoxazines (PBZs) are phenolic resins and types of high-performance thermosetting polymers [21–24]. These kinds of phenolic resins have several attractive properties: good solvent-resistance, corrosion-resistance, and flame-retardancy; ease of processability; chemical stability; good mechanical properties; low hygroscopicity; low surface free energies; high carbon residue rates; low dielectric

* Corresponding author at: Department of Materials and Optoelectronic Science, Center of Crystal Research, National Sun Yat-Sen University, Kaohsiung, Taiwan.
E-mail address: kuosw@faculty.nsysu.edu.tw (S.-W. Kuo).

https://doi.org/10.1016/j.mtcomm.2020.101111
Received 5 March 2020; Received in revised form 30 March 2020; Accepted 30 March 2020
Available online 10 April 2020
2352-4928/

constants; high glass transition temperatures (T_g); and no release of small molecules during their thermal curing polymerization [25–28]. PBZ resins are readily synthesized through thermal ring opening polymerization (ROP) from benzoxazine monomers, which are themselves prepared through Mannich condensation by phenols and amines with paraformaldehyde in the presence or absence of a solvent [29–35]. PBZ resins differ from other traditional phenolic resins because the presence of N atoms in the main chains of the PBZ after thermal curing of the benzoxazine units provides the potential for hydrogen bonding with OH groups, thereby increasing the hydrophobicity of such materials [36–38]. Although PBZ resins can display outstanding properties, these properties can be improved further through processing. Two main approaches have been developed for the modification of benzoxazines: (i) changing the chemical structures of the amines and phenols to present nitrile, hydroxyalkyl, alkyl, carboxyl, or propargyl groups from the benzoxazine monomers and (ii) blending or copolymerizing the benzoxazine monomers with polyhedral oligomeric silsesquioxane (POSS), carbon nanotubes, nanoclay, polydimethylsiloxane (PDMS), and graphene [39–42]. Many previous reports describe the preparation of highly porous and highly thermally stable N-doped porous carbons from PBZ matrices in three steps: thermal curing, carbonization, and KOH chemical activation. For example, Hao et al. prepared N-doped porous carbons by using the polymer poly(benzoxazine-*co*-resol) as a precursor; these materials exhibited excellent CO_2 capture [43]. Furthermore, the Li group prepared N-containing porous carbons by the nitrile-functionalized benzoxazine monomer [44]. We obtained N-doped microporous carbons (NMCs) by the nitrile-functionalized benzoxazine matrix, which we prepared through the reaction of 4-cyanophenol, TriPh-3NH_2, and CH_2O; the CO_2 uptake ability of this BZCN-A microporous carbon was 2.82 mmol g^{-1} [45].

In this present study, we prepared the two new benzoxazine monomers BZAPh and BZACN, each containing azobenzene units, through Mannich condensations of TriPh-3NH_2 and $(CH_2O)_n$ with 4-phenylazophenol and 4-[(4-hydroxyphenyl)diazenyl]benzonitrile (AzoOHCN), respectively. We used NMR spectroscopy, (temperature-dependent) FTIR spectroscopy, high-resolution Fourier transform mass spectrometry (HR-FT-MS), DSC, and TGA to examine the chemical structures and thermal curing behavior of these two monomers and their thermal stability before and after thermal curing at various temperature. We then employed carbonization and KOH activation chemical process of the polymers poly(BZAPh) and poly(BZACN) at 800 °C to obtain the N-doped-porous carbon materials poly(BZAPh)-A and poly (BZACN)-A, respectively. We investigated the specific surface areas, porous structures, surface morphologies, chemical compositions, thermal stabilities, and CO_2 uptake abilities of the highly N-doped hierarchically porous carbons derived from the benzoxazine monomers BZAPh and BZACN through Raman spectroscopy, XRD, XPS, TEM, the BET method, TGA, and CO_2 adsorption measurements. This report is the first to describe the effect of the incorporation of azobenzene units into the benzoxazine matrix on the properties of the resulting N-doped carbon materials, including their CO_2 capture abilities.

2. Experimental section

2.1. Materials

Phloroglucinol, *N*,*N*-dimethylformamide (DMF), potassium carbonate (K_2CO_3), 10 % palladium on activated carbon (Pd/C, 10 wt%), 4-phenylazophenol, and anhydrous magnesium sulfate ($MgSO_4$) were purchased from Sigma–Aldrich. Hydrazine monohydrate ($NH_2NH_2{\cdot}H_2O$), hexane, 1-fluoro-4-nitrobenzene, absolute ethanol (EtOH, 99.9 %), 1,4-dioxane, paraformaldehyde, tetrahydrofuran (THF), acetonitrile (CH_3CN), hydrochloric acid (37 %), and dichloromethane (CH_2Cl_2) were purchased from Acros. The synthesis of TriPh-3NH_2 was performed according to a previously reported method, as summarized in Scheme S1 and Fig. S1 and S2 [45,46].

2.2. AzoOHCN [Scheme S2] [47]

In two-neck round-bottom flask (250 mL) under a N_2 atmosphere, 4-cyanoaniline (5.00 g, 42.3 mmol) was dissolved in hydrochloric acid (10 mL) and water (10 mL) and then the solution was cooled to 0 °C with stirring. A solution of $NaNO_2$ (2.90 g, 42.3 mmol) in water (20 mL) was added slowly to the reaction mixture at 0 °C to form a solution of the diazonium salt. A solution of phenol (3.98 g, 42.3 mmol) in 10 wt% aqueous NaOH (28 mL) was cooled to 5 °C and added to the cold solution of the diazonium salt. The mixture was left for 6 h at 0 °C and then acidified with aqueous HCl to form an orange solid, which was filtered off and washed many times with water. The orange powder was purified through column chromatography (EtOAc/hexane, 1:3) to give AzoOHCN as an orange powder (7.00 g, 64 %). FTIR (KBr, cm^{-1}): 3388 (OH stretching), 3070 (CH− aromatic), 2227 (CN stretching). ^{1}H NMR (500 MHz, DMSO-d_6, δ, ppm, Fig. S3): 10.60 (1H, s, OH), 6.98 (2H, d), 7.80 (2H, d), 7.93 (4H, t). ^{13}C NMR (125 MHz, DMSO-d_6, δ, ppm, Fig. S4): 162.42, 154.99, 145.88, 134.74, 126.31, 123.92, 116.82 (CN).

2.3. BZAPh

A solution of TriPh-3NH_2 (1.00 g, 2.51 mmol), paraformaldehyde (0.45 g, 15.0 mmol), and 4-phenylazophenol (1.49 g, 7.52 mmol) in 1,4-dioxane (50 mL) was heated under reflux at 110 °C for 24 h under a N_2 atmosphere in a round-bottom flask (100 mL) equipped with a condenser and magnetic stirrer. The mixture was cooled to room temperature and then the 1,4-dioxane was evaporated under reduced pressure at 50 °C. A small amount of CH_2Cl_2 was added to dissolve the residue, then hexane (300 mL) was added to precipitated BZAPh as an orange solid (1.00 g, 60 %). FTIR (KBr, cm^{-1}): 3057 (CH aromatic), 1602 (C═C stretching), 1233 (C−OC− asymmetric stretching), 930 (oxazine ring). ^{1}H NMR (500 MHz, DMSO-d_6, δ, ppm): 7.99–6.04 (ArCH), 5.52 (OCH_2N), 4.74 ($ArCH_2N$). ^{13}C NMR (125 MHz, DMSO-d_6, δ, ppm): 161.81–113.54 (aromatic), 80.32 (OCH_2N), 49.24 ($ArCH_2N$). HR-FT-MS: calcd. for $C_{66}H_{52}N_9O_6$: *m/z* 1065.4; found: 1066.4 (Fig. S5).

2.4. Bzacn

A solution of TriPh-3NH_2 (1.00 g, 2.51 mmol), paraformaldehyde (0.45 g, 15.0 mmol), and AzoOHCN (1.68 g, 7.52 mmol) in 1,4-dioxane (50 mL) was heated at 110 °C for 24 h under N_2 atmosphere in a round-bottom flask (100 mL) equipped with a condenser and a magnetic stirrer. The mixture was cooled to room temperature and then the solvent was evaporated under reduced pressure. A small amount of CH_2Cl_2 was added to dissolve the residue, and then hexane (300 mL) was added to precipitate BZACN as an orange solid (1.0 g, 60 %). FTIR (KBr, cm^{-1}): 3051 (CH aromatic), 1597 (C═C stretching), 1227 (C−OC− asymmetric stretching), 925 (oxazine ring). ^{1}H NMR (500 MHz, DMSO-d_6, δ, ppm,): 7.82–6.06 (ArH), 5.51 (OCH_2N), 4.74 ($ArCH_2N$). ^{13}C NMR (125 MHz, DMSO-d_6, δ, ppm): 162.93–113.12 (aromatic), 80.49 (OCH_2N), 40.29 ($ArCH_2N$). HR-FT-MS: calcd. for $C_{69}H_{49}N_{12}O_6$: *m/z* 1140.38; found: 1141.39 (Fig. S6).

2.5. Thermal curing polymerization of BZAPh and BZACN

A desired amount of the BZAPh or BZACN monomer was charged in an aluminum pan and placed in an oven and heated at various temperatures (110, 150, 180, 210, and 250 °C; 2 h at each temperature) to afford poly(BZAPh) and poly(BZACN) as a black powder.

2.6. NMCs derived from monomers BZAPh and BZACN

A desired amount of the monomer BZAPh or BZACN (2.00 g) was polymerized in an oven for 5 h at 250 °C. The sample was then calcined in a tubular furnace, by heating at a rate of 5 °C min^{-1} under a N_2 atmosphere and then at 600 °C for 2 h. The black sample was mixed in

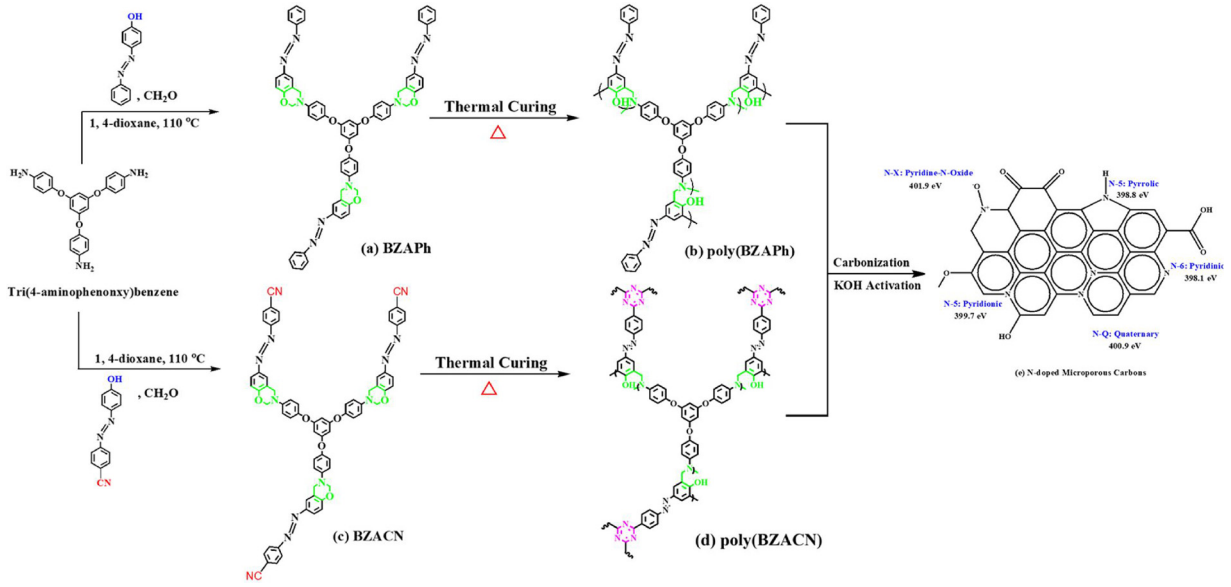

Scheme 1. Syntheses of (a) BZAPh, (b) poly(BZAPh), (c) BZACN, (d) poly(BZACN), and (e) the NMCs.

aqueous KOH and stirred overnight at 25 °C. The water was evaporated under reduced pressure at 120 °C for 24 h under vacuum. Then, the activated sample was transferred into a tubular furnace and heated at a rate of 5 °C min^{-1} under a N_2 atmosphere and then at 800 °C for 8 h to afford an NMC (1.00 g, 50 %).

3. Results and discussion

3.1. Synthesis of the monomers BZAPh and BZACN

Scheme 1 presents the syntheses of the monomers BZAPh and BZACN; their structures were confirmed using FTIR and NMR spectroscopies and high-resolution mass spectrometry. Fig. 1 displays the FTIR spectra of AzoOHCN, TriPh-3NH_2, BZAPh, and BZACN. The FTIR spectrum of AzoOHCN [Fig. 1(a)] features three major signals at 3388, 3070, and 2227 cm^{-1}, representing its phenolic OH, aromatic CH, and nitrile units, respectively. The characteristic absorption signals for the amino groups of TriPh-3NH_2 appeared at 3400 and 3200 cm^{-1} [Fig. 1(b)]. The characteristic absorptions bands for BZAPh appeared at 3057, 1233, and 930 cm^{-1} [Fig. 1(c)] and for BZACN at 3051, 1227, and 925 cm^{-1} [Fig. 1(d)], representing their aromatic CH, asymmetric C—OC— stretching, and benzoxazine-related bands, respectively. The absence of signals at 3388 cm^{-1} (representing phenolic OH groups) in the spectra of both BZAPh and BZACN monomers and the appearance a signal at 2225 cm^{-1} (representing a cyano group) in the spectrum of the BZACN monomer, confirmed the successful syntheses of both monomers in high purity and yield.

Fig. 2 displays the ^1H NMR spectra of TriPh-3NH_2, BZAPh, and

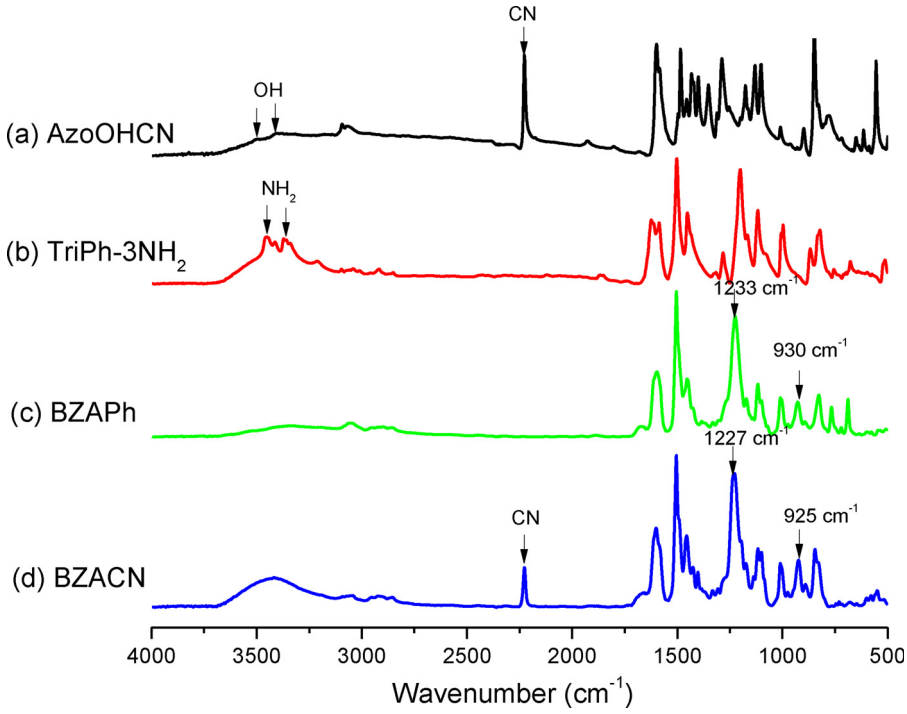

Fig. 1. FTIR spectra of (a) AzoOHCN, (b) TriPh-3NH_2, (c) BZAPh, and (d) BZACN.

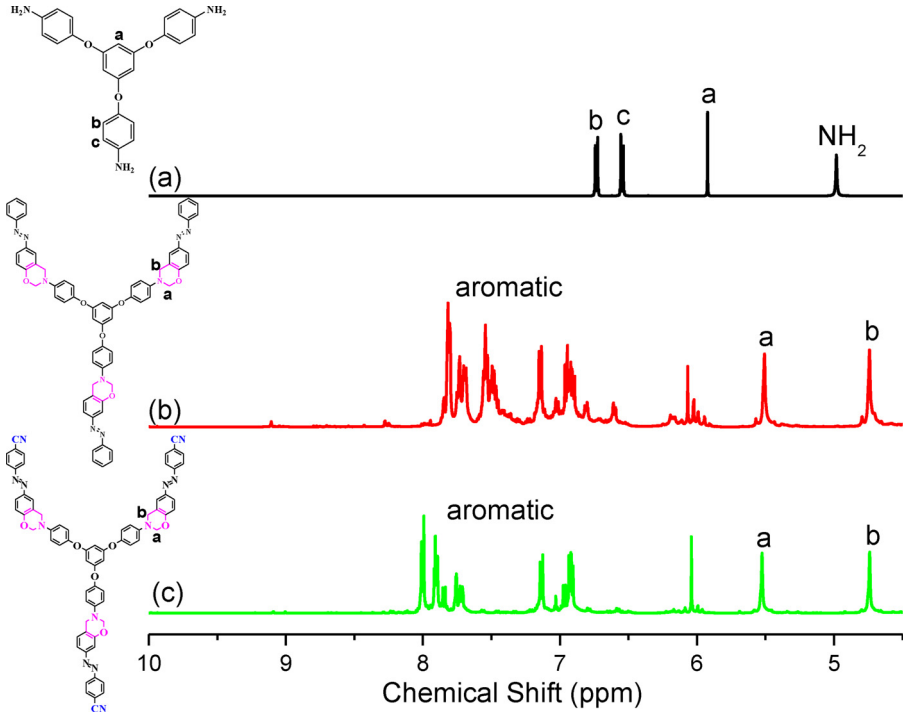

Fig. 2. ^{1}H NMR spectra of (a) TriPh-3NH$_2$, (b) BZAPh, and (c) BZACN.

BZACN in DMSO-d$_6$. The ^{1}H NMR spectrum of TriPh-3NH$_2$ [Fig. 2(a)] features signals at 6.72–5.92 ppm that we assign to aromatic protons and at 4.98 ppm for the NH$_2$ groups. The ^{1}H NMR spectrum of BZAPh [Fig. 2(b)] contains two sharp peaks centered at 4.74 and 5.51 ppm and that for BZACN [Fig. 2(c)] features signals centered at 4.74 and 5.52 ppm, in each case representing the ArCH$_2$N and OCH$_2$N units in their oxazine rings.

Fig. 3 presents the ^{13}C NMR spectra of TriPh-3NH$_2$, BZAPh, and BZACN. Signals for two carbon nuclei appeared at 80.32 and 49.24 ppm for the ArCH$_2$N and OCH$_2$N units of BZAPh, with aromatic signals appearing in the range from 161.81–113.54 ppm [Fig. 3(b)]. Similar characteristic signals for BZACN appeared at 80.49 and 49.29 ppm. In addition, the signal of the carbon nucleus of the nitrile group appeared at 113.11 pm in the spectrum of BZACN. Together, these spectra confirmed the syntheses of the monomers BZAPh and BZACN.

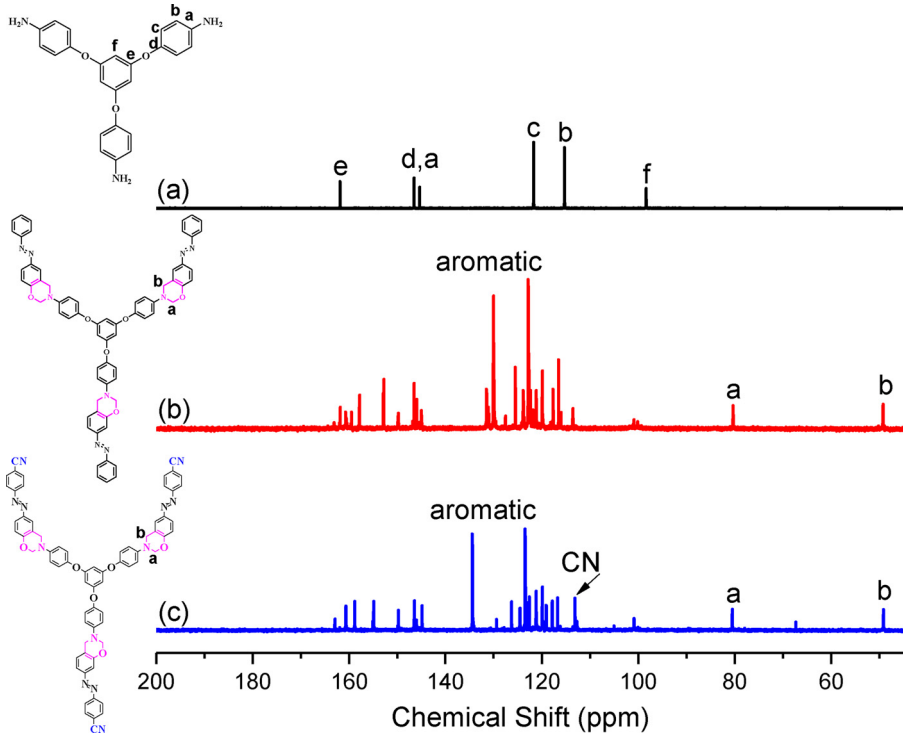

Fig. 3. ^{13}C NMR spectra of (a) TriPh-3NH$_2$, (b) BZAPh, and (c) BZACN.

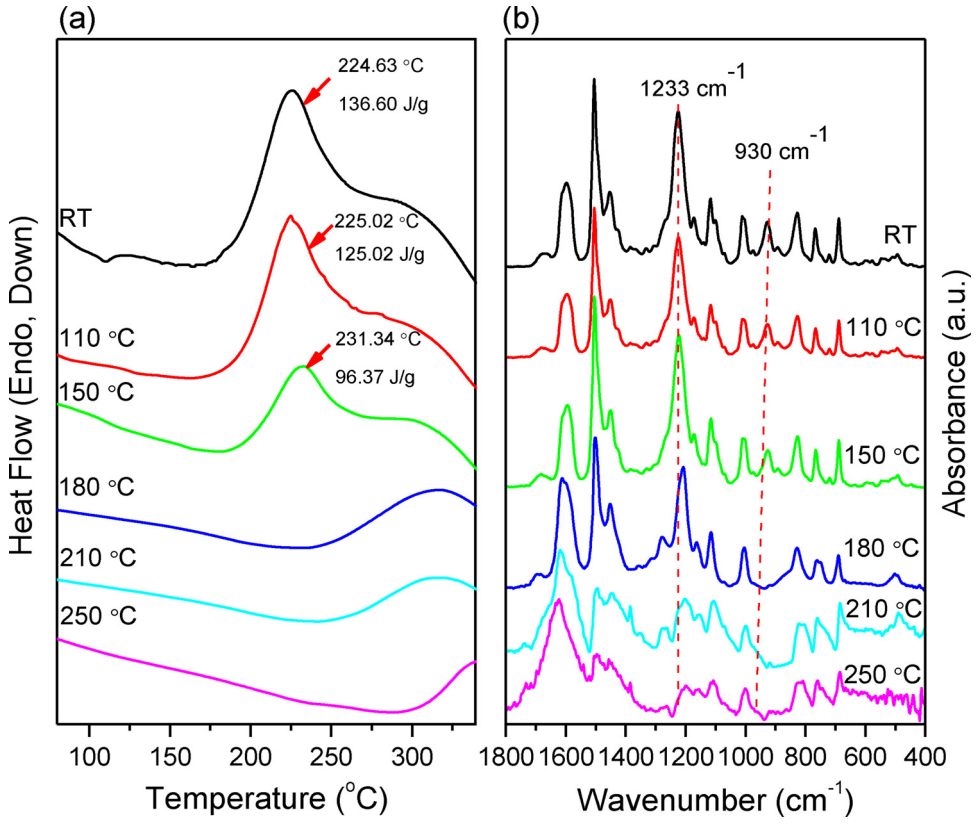

Fig. 4. (a) DSC and (b) FTIR spectral analyses of BZAPh before and after thermal curing from room temperature to 250 °C.

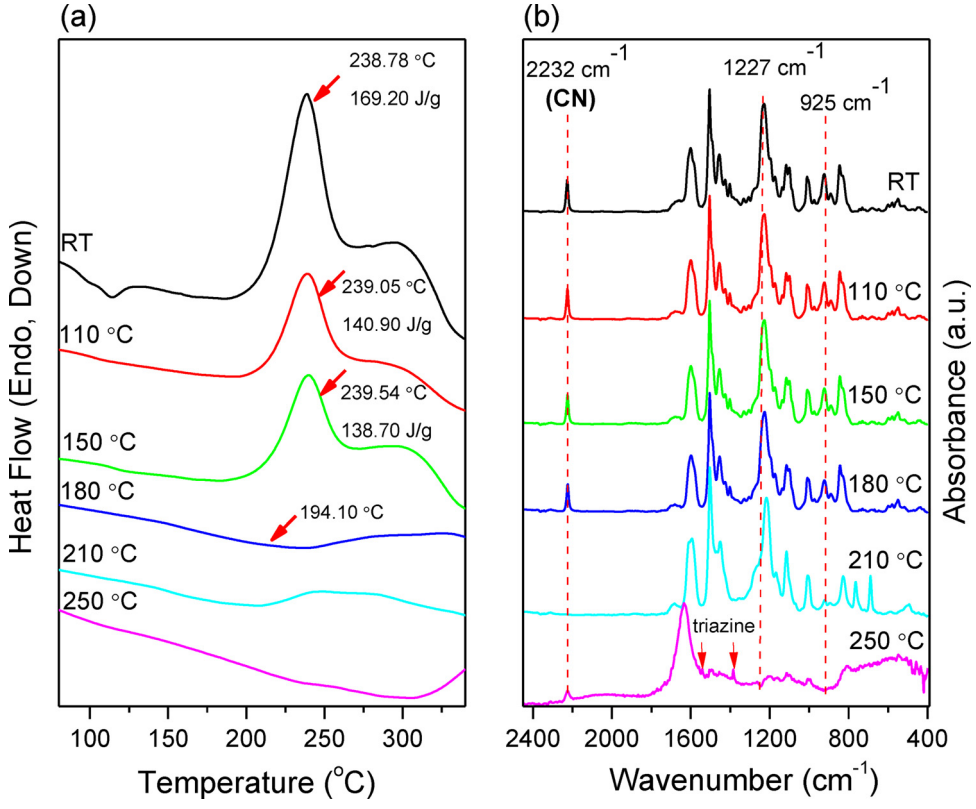

Fig. 5. (a) DSC and (b) FTIR spectral analyses of BZACN before and after thermal curing from room temperature to 250 °C.

3.2. Thermal curing polymerization of the monomers BZAPh and BZACN

We used DSC (Fig. 4) and FTIR spectroscopy (Fig. 5) to examine the thermal ROP of BZAPh and BZACN. Fig. 4(a) displays the DSC profiles of the uncured BZAPh and the products of its polymerization at temperatures from 110 to 250 °C. The uncured BZAPh monomer displayed a maximum exothermic curing peak at 224 °C with a reaction heat of 136 J g^{-1} and a melting temperature of 110 °C. After thermal curing of BZAPh at temperatures of 110 and 150 °C, the maximum exothermic curing peaks were centered at 225 and 231 °C, respectively, with reaction heats of 125 and 69 J g^{-1}, respectively. Further thermal curing at 180 °C caused the maximum exothermic curing peak to disappear completely, suggesting complete ROP of the oxazine units and form poly(BZAPh) with high crosslinking density. Fig. 4(b) presents corresponding FTIR spectra of the uncured BZAPh and its products from thermal curing. The signals of the benzoxazine moiety in BZAPh appeared at 1233, 1170, and 930 cm^{-1}, representing its C–O–C, C–N–C, and benzoxazine units, respectively. All these characteristic absorption signals for the benzoxazine ring in the monomer disappeared completely after curing the monomer at temperatures from 180 to 250 °C.

Fig. 5 displays the DSC thermograms of the BZACN monomer, which provided a sharp exothermic peak at 238 °C and a reaction heat of 169 J g^{-1}. Again, the thermal curing peak disappeared completely after increasing the thermal curing temperature from 180 to 250 °C. The BZACN monomer possessed a melting temperature of 114 °C; the poly (BZACN) obtained after thermal curing at 180 °C had a glass transition temperature of 194 °C. Interestingly, the exothermic curing peaks for the oxazine units in BZAPh and BZACN [Figs. 4(a) and 5(a)] appeared at lower temperatures than that for the typical Pa-type monomer 3-phenyl-3,4-dihydro-2*H*-benzooxazine (263 °C), presumably because the azobenzene units in both monomers and the CN unit in BZACN acted as catalysts for ROP of these benzoxazine units [48,49]. The characteristic FTIR spectral absorption signals for the benzoxazine unit in the BZACN monomer completely disappeared after thermal treatment at 210 and 250 °C [Fig. 5(b)], is good agreement with the results of the DSC analysis. The absorption band for the CN unit at 2232 cm^{-1} disappeared after thermal curing at 210 or 250 °C, with two new characteristic absorptions at 1543 and 1385 cm^{-1}, confirming the trimerization of the CN groups at these temperatures to form extended two-dimensional (2D) frameworks (triazine covalent frameworks) of the poly(BZACN) type with high crosslinking density.

We used TGA analysis (Fig. 6) under a N_2 atmosphere to investigate the thermal stabilities of the uncured monomers BZAPh and BZACN and the products of their polymerization after thermal curing at various temperatures (from 110 to 250 °C). Fig. 6(a) and (b) reveal that, before thermal curing, the monomers BZAPh and BZACN exhibited decomposition temperatures (T_{d10}; 10 % weight-loss temperatures) of 270 and 267 °C, respectively, and char yields (residual weight remaining at 800 °C) of 53.3 and 61.0 wt%, respectively. As expected, after increasing the thermal curing temperature, the thermal decomposition temperatures and char yields of increased to 410 °C and 66.1 wt%, respectively, for poly(BZAPh) and to 404 °C and 66.3 wt%, respectively, for poly (BZACN), consistent with increasing crosslinking densities after the ROPs of the benzoxazine rings to form three-dimensional (3D) structures in both PBZ cases. Furthermore, poly(BZACN) displayed a higher value of T_d (404 °C) than that of the BZCN-type PBZ (393 °C), presumably because of the presence of the azobenzene moiety in the BZACN monomer. In addition, poly(BZACN) provided a higher char yield (66.3 wt%) than that of poly(BZAPh) (66.1 wt%), presumably because of the formation of an additional 2D framework of triazine rings [44,45].

3.3. Characterization of NMCs derived from monomers BZAPh and BZACN

We prepared NMCs derived from the poly(BZAPh) and poly(BZACN) by applying carbonization and KOH activation processes, as detailed in the Experimental section and presented in Scheme 1(e). The porous structures and properties, including the BET surface areas and pore size distributions, of poly(BZAPh)-A and poly(BZACN)-A were examined through N_2 adsorption/desorption experiments at 77 K (Fig. 7, Table 1). As displayed in Fig. 7(a) and (c), the isothermal curves of poly(BZAPh)-A and poly(BZACN)-A both featured rapid increases in absorption at low values of P/P_0 (< 0.05), indicating that both of these NMCs were microporous carbon materials that provided type-I isotherms. Furthermore, the BET surface areas of poly(BZACN)-A (942 m^2 g^{-1}) is higher than that poly(BZAPh)-A (523 m^2 g^{-1}) which is attributed to the presence 2D framework of triazine rings in poly(BZACN) which could provide abundant micropores, increase of micropore area and micropore volume in poly(BZACN)-A after carbonization and KOH activation [44]. In addition, the pore size distributions, calculated using nonlocal density functional theory [Fig. 7(b) and (d)], revealed that the average pore sizes for the poly(BZAPh)-A and poly(BZACN)-A microporous carbon materials were 0.433 and 1.40 nm; these results were consistent with the TEM images in Fig. 7(c) and (e). Also, SEM images [Fig. S7(a) and (b)] indicate that poly(BZAPh)-A and poly(BZACN)-A had pore structure.

We used powder XRD to investigate the degrees of graphitization of our prepared NMCs poly(BZAPh)-A and poly(BZACN)-A (Fig. S8). The patterns of poly(BZAPh)-A and poly(BZACN)-A both featured two broad diffraction peaks located at values of 2θ of 25 and 44°, which we assigned to the (002) and (100) planes of irregular and amorphous carbon and graphitic carbon, respectively [50]. The intensity of the diffraction signal at a value of 2θ of 44° for poly(BZACN)-A was stronger than that for poly(BZAPh)-A, presumably because the presence of CN groups led to the formation of more of a perfect regular carbon. The XPS profiles of our microporous carbon materials poly(BZAPh)-A and poly(BZACN)-A (Fig. S9) revealed three distinct peaks centered at 284, 400, and 530 eV, corresponding to C, N, and O atoms on their surfaces. We fitted the XPS data for the N and O atoms on the surface of our synthesized poly (BZAPh)-A and poly(BZACN)-A microporous carbon materials to investigate their degrees of graphitization (Fig. 8, Table 2). According to the curve fitting analyses, as presented in Fig. 8(c) and (d) and in Scheme 1(e), four types of N-containing species were present on the surfaces of the microporous carbon materials poly(BZAPh)-A and poly (BZACN)-A: oxidized nitrogen species (N–X, near 403 eV), quaternary nitrogen species (N-3, near 401 eV), pyridonic or pyridone nitrogen species (N-6, near 400 eV), and pyridinic nitrogen species (N-5, near 398 eV). The O-containing species on the surface of these microporous carbon materials included adsorbed H_2O (535.9 eV), CO—H units (534.2 eV), C—O units (533.3 eV), CO═ units (532.3 eV), and quinone species (531.3 eV), according to the results of fitting the O1s spectra [Fig. 8(a) and (b)] [11,45,51]. As expected, after activation of poly (BZAPh) and poly(BZACN), the N- and O-atom contents were 2.6 and 19.3 wt%, respectively, for poly(BZAPh)-A and 4.6 and 23 wt%, respectively, for poly(BZACN)-A. The N-5 concentration (58.0 %) in poly (BZACN)-A was higher than that in poly(BZAPh)-A (48.3 %) because of the presence of extra CN groups in poly(BZACN). In addition, our NMCs derived from BZAPh and BZACN contained higher fractions of N-5, N-6, and oxygen units when compared with previously reported NMC materials [11,16,45,52]. Therefore, we expected that these new materials might be useful for energy storage and CO_2 uptake.

Fig. 9 presents the Raman spectra of our microporous carbon materials poly(BZAPh)-A and poly(BZACN)-A. For both materials, two characteristic peaks appeared at 1350 cm^{-1} (corresponding to the D band, representing imperfect and disarrayed structures derived from turbostratic carbon layers) and 1599 cm^{-1} (corresponding to the G band, representing the vibration of sp^2-hybridized carbon atoms) [45,51]. We calculated the intensity ratios for the D- and G-bands (I_D/I_G) to characterize the degrees of graphitization of these carbon materials. The value of I_D/I_G for poly(BZACN)-A (0.95) was lower than that of poly(BZAPh)-A (0.99), suggesting that poly(BZACN)-A possessed a regular microporous structure, presumably because of the formation of

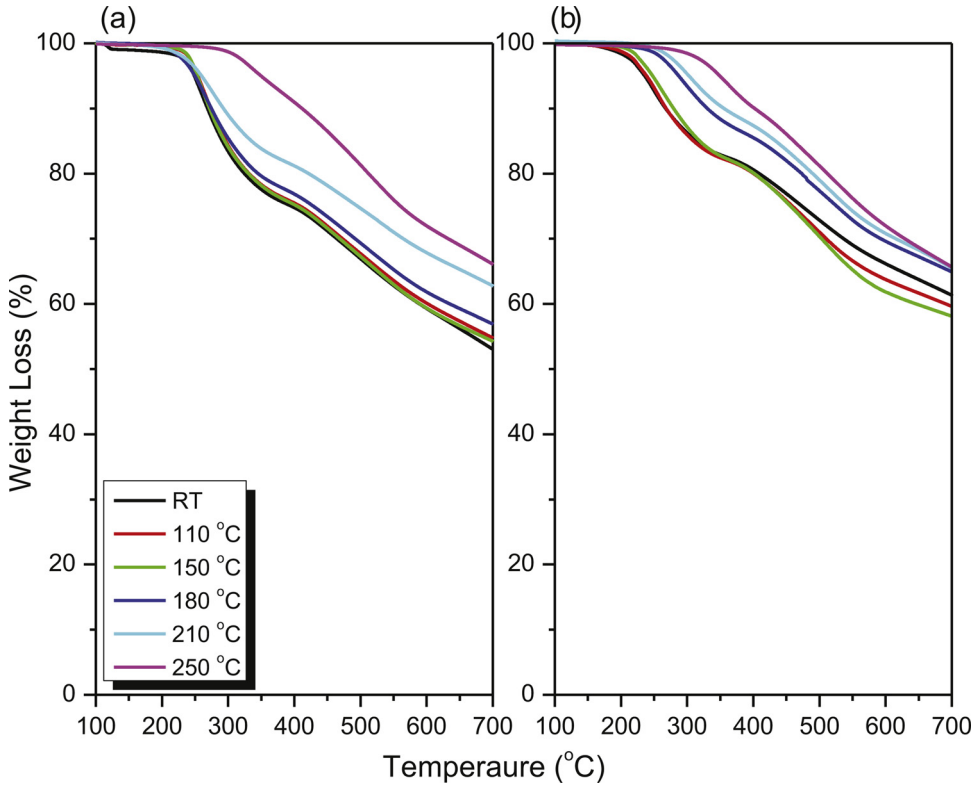

Fig. 6. TGA profiles of the monomers (a) BZAPh and (b) BZACN, recorded before and after curing at temperatures from 25 to 250 °C.

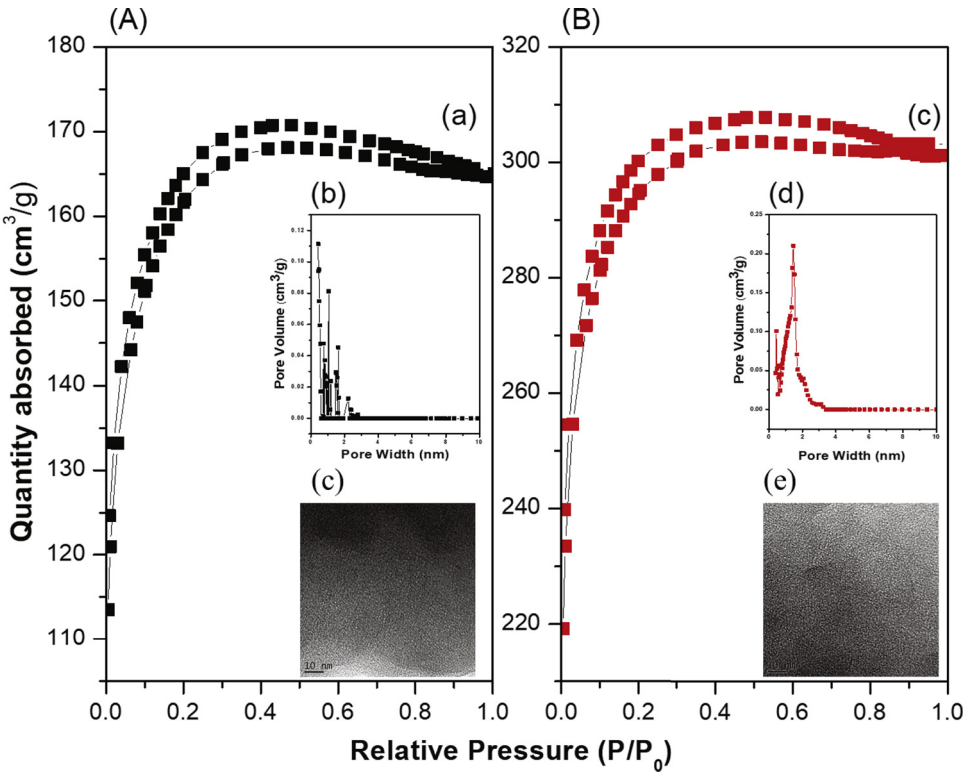

Fig. 7. (a, c) Nitrogen adsorption/desorption isotherms, (b, d) pore size distribution, and (c, e) TEM images of (A) poly(BZAPh)-A and (B) poly(BZACN)-A.

an additional 2D framework of triazine rings at high temperature. These findings are consistent with the results of the XRD and XPS analyses. We used TGA to measure the thermal stabilities of our microporous carbon materials poly(BZAPh)-A and poly(BZACN)-A (Fig. S10, and Table 1). Interestingly, poly(BZAPh)-A and poly(BZACN)-A had similar values of T_{d10} (588 °C) and similar char yields (92 wt%). Thus, both poly (BZAPh)-A and poly(BZACN)-A had outstanding thermal stabilities after chemical activation with KOH.

Table 1
Thermal properties, surface areas, XPS data, and CO_2 uptake behavior of the monomers BZAPh and BZACN and the products obtained after thermal curing, carbonization, and activation.

Samples	T_{d10} (°C)	Char yield (wt %)	XPS analysis (%) C	O	N	S_{micro} (m^2 g^{-1})	CO_2 uptake (mmol g^{-1}) 298 K	273 K
BZAPh	250	47.3	–	–	–	–	–	–
BZACN	236	57.2	–	–	–	–	–	–
poly(BZAPh)	349	61.9	–	–	–	–	–	–
poly(BZACN)	350	61.1	–	–	–	–	–	–
poly(BZAPh)-A	588	92.0	79.0	19.3	2.6	522	3.00	5.25
poly(BZACN)-A	588	92.0	71.6	23.0	4.6	942	4.00	8.13

3.4. CO_2 capture of poly(BZAPh)-A and poly(BZACN)-A

As mentioned above, we suspected that our new NMCs could be useful for CO_2 uptake because they contained higher contents of N-5, N-6, and oxygen units when compared with those of other previously reported N-rich carbon materials [11,15,16,45,52,53]. Fig. 10(a) and (b) display the equilibrium CO_2 isotherms of the microporous carbon materials poly(BZAPh)-A and poly(BZACN)-A, recorded at 298 and 273 K, respectively. The degrees of CO_2 capture of poly(BZACN)-A at 298 and 273 K were 4.00 and 8.13 mmol g^{-1}, respectively; for poly(BZAPh)-A, these values were 3.30 and 5.25 mmol g^{-1}, respectively. The superior performance of poly(BZACN)-A presumably arose because of its higher surface (942 m^2 g^{-1}) and higher content of N-containing species (58 %), and large pore diameter (1.40 nm) relative to those of poly(BZAPh)-A (522 m^2 g^{-1} 48.3 % and 0.433 nm, respectively), arising from the extra triazine units derived from the BZACN monomer. As previously reported, a higher N-atom concentration in a microporous carbon material enhances its adsorption ability and efficiency toward acidic CO_2 gas [11,16,45,52,53]. Previously, we prepared corresponding materials poly(BZPh)-A and poly(BZCN)-A lacking azobenzene units; their degrees of CO_2 uptake were only 1.44 and 2.82 mmol g^{-1}, respectively [45]. Table S1 compares the CO_2 capture abilities of poly(BZAPh)-A and poly(BZACN)-A with those of other previously reported N-doped carbon materials derived from PBZ matrices [52,54]. Both poly(BZAPh)-A and poly(BZACN)-A exhibited excellent CO_2 uptake behavior, superior to those of other types of N-doped carbon materials derived from PBZ, when measured at the same temperatures (298 and 273 K). Our azobenzene-and-nitrile-functionalized PBZ appears to be a good candidate material for CO_2 adsorption.

4. Conclusions

We have prepared to NMCs derived from the monomers BZAPh and BZACN. DSC revealed that the thermal curing temperatures for both monomers were lower than that of a typical Pa-type benzoxazine monomer, presumably because of the presence of azobenzene units in both monomers and the presence of a CN unit in the monomer BZACN; these units could act as catalytic sites for the ROP of the benzoxazine units. The products obtained after thermal curing of the monomers possessed high thermal stability, due to high cross-linking densities, as determined using TGA. After performing carbonization and KOH activation processes, the microporous carbon material poly(BZACN)-A displayed CO_2 capture ability greater than that of poly(BZAPh)-A when measured at the same temperature. The superior CO_2 capture of poly(BZACN)-A arose because of its higher surface area and higher content of N-containing species in its structure. Furthermore, the CO_2 capture abilities of poly(BZAPh)-A and poly(BZACN)-A were superior to those of previously reported N-doped carbon materials synthesized from PBZ matrices, when measured at the same temperatures (298 and 273 K).

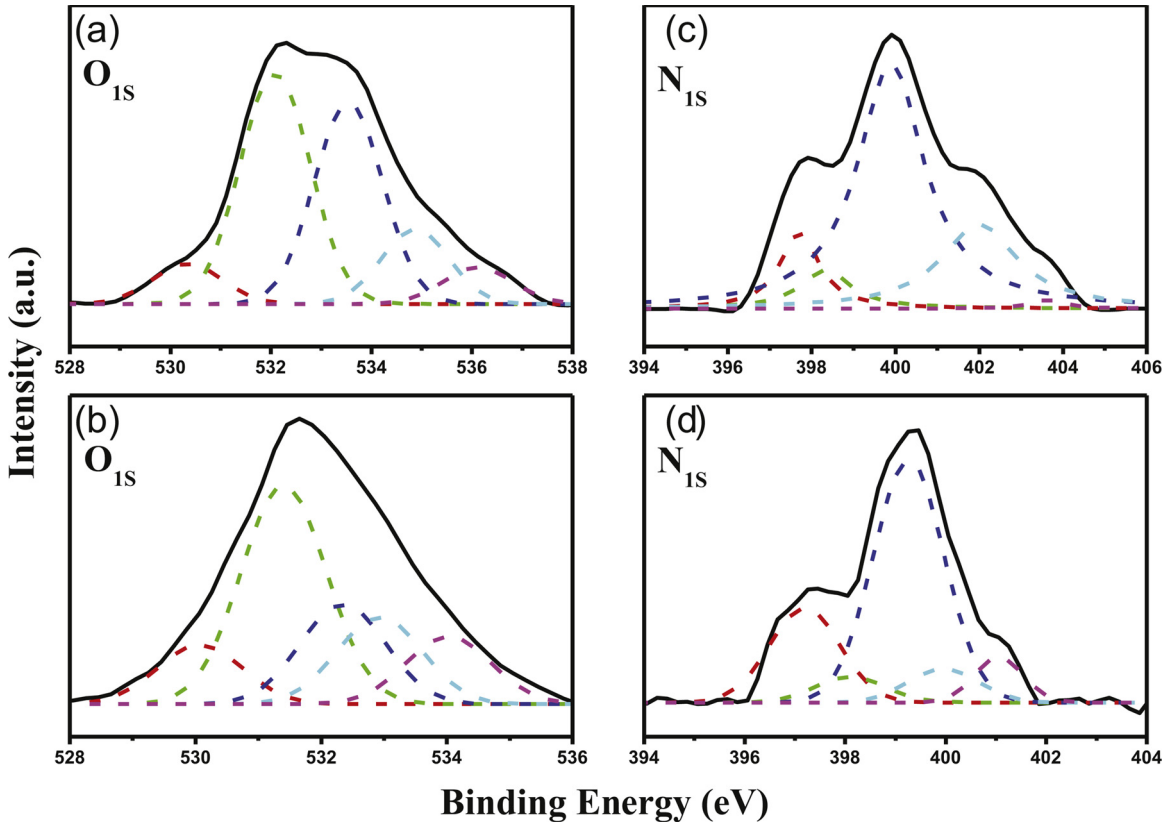

Fig. 8. XPS spectra (O1s and N1s orbitals) of (a, c) poly(BZAPh)-A and (b, d) poly(BZACN)-A.

Table 2
Curve-fitting data for the area fractions derived from the N1s and O1s spectra of the microporous carbons poly(BZAPh)-A and poly(BZACN)-A.

Samples	N species				O species				
	N-6	N-5	N-Q	N-X	Quinone	C = O	C-O	C-OH	H_2O
poly(BZAPh)-A	6.30	48.30	29.84	15.56	11.85	16.34	31.27	22.06	18.48
Poly(BZACN)-A	9.30	58.00	22.70	10.00	10.29	13.15	38.06	24.21	14.29

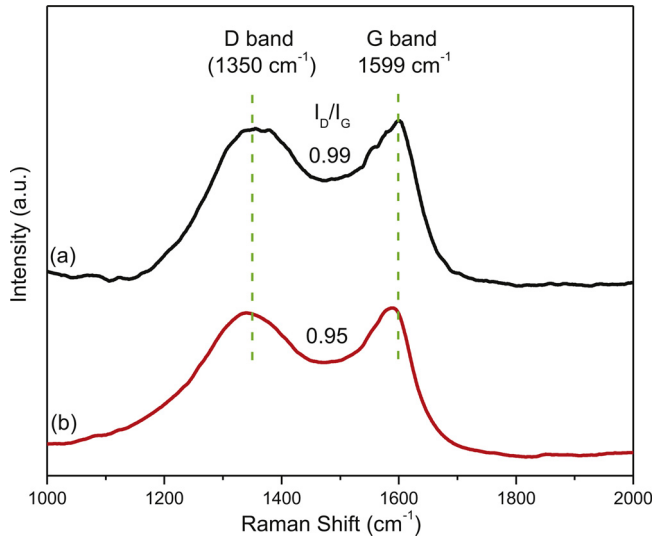

Fig. 9. Raman spectra of (a) poly(BZAPh)-A and (b) poly(BZACN)-A.

Author Statement

M.G.M., M.Y.T. W.C.S. and A.F.M.M. did the experiment, C.F.W, H.C.H, T.C help to design the CO2 uptake, L.D and T.C. help to design the CV analyses, and S.-W.K. contributed to the literature review and to the writing of this paper.

Declaration of Competing Interest

The authors declare that they have no known competing financial interests or personal relationships that could have appeared to influence the work reported in this paper.

Acknowledgment

This study was supported financially by the Ministry of Science and Technology, Taiwan, under contracts MOST 108-2638-E-002 -003 -MY2, 106-2221-E-110-067-MY3, 108-2221-E-110-014-MY3, and 108-2218-E-110-013-MY3. This work also supported by the National Natural Science Foundation of China (51773214).

Appendix A. Supplementary data

Supplementary material related to this article can be found, in the online version, at doi:https://doi.org/10.1016/j.mtcomm.2020.101111.

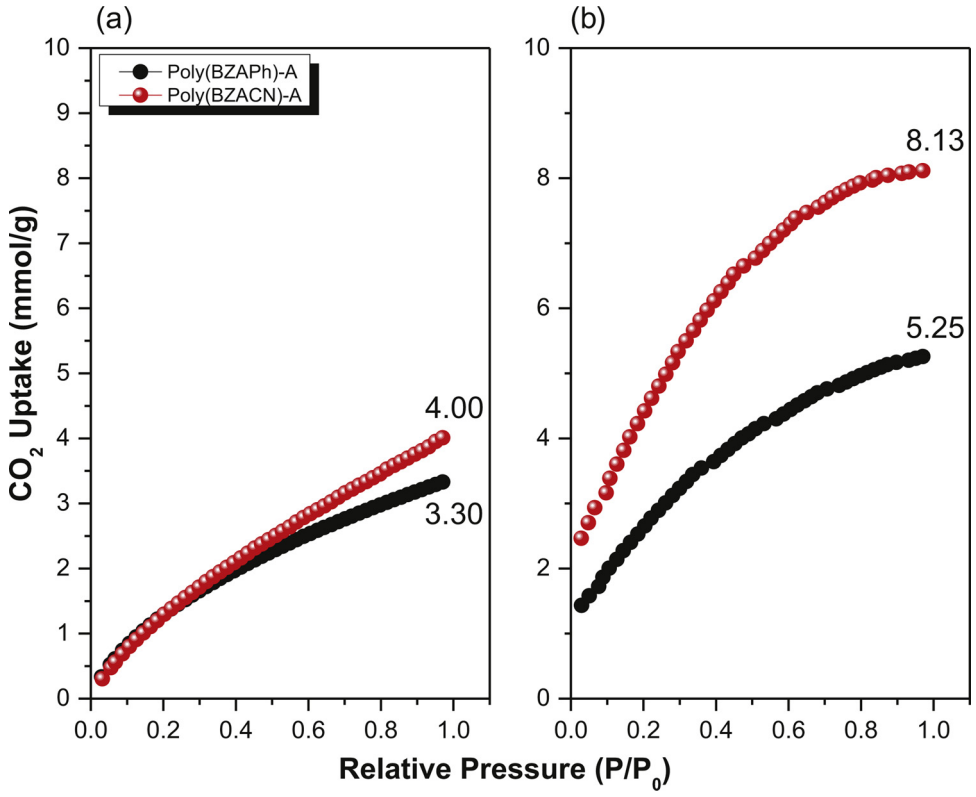

Fig. 10. CO_2 uptake profiles of poly(BZAPh)-A and poly(BZACN)-A, recorded at (a) 298 and (b) 273 K.

References

[1] Y. Wan, D.Y. Zhao, On the controllable soft-templating approach to mesoporous silicates, Chem. Rev. 107 (2007) 2821–2860.
[2] A.D. Roberts, X. Li, H. Zhang, Porous carbon spheres and monoliths: morphology control, pore size tuning and their applications as Li-ion battery anode materials, Chem. Soc. Rev. 43 (2014) 4341–4356.
[3] M. Li, C. Liu, H. Cao, H. Zhao, Y. Zhang, Z. Fan, KOH self-templating synthesis of three-dimensional hierarchical porous carbon materials for high performance supercapacitors, J. Mater. Chem. A 2 (2014) 14844–14851.
[4] J.G. Li, Y.D. Lin, S.W. Kuo, From microphase separation to self-organized mesoporous phenolic resin through competitive hydrogen bonding with double-crystalline diblock copolymers of poly(ethylene oxide-b-ε-caprolactone), Macromolecules 44 (2011) 9295–9309.
[5] M. Kopec', M. Lamsona, R. Yuan, C. Tang, M. Kruk, M. Zhong, K. Matyjaszewskia, T. Kowalewski, Polyacrylonitrile-derived nanostructured carbon materials, Prog. Polym. Sci. 92 (2019) 89–134.
[6] W.C. Chen, M.M.M. Ahmed, C.F. Wang, C.F. Huang, S.W. Kuo, Highly thermally stable mesoporous Poly(cyanate ester) featuring double-decker–shaped polyhedral silsesquioxane framework, Polymer 185 (2019) 121940–121950.
[7] J. Gong, X. Chen, T. Tang, Recent progress in controlled carbonization of (waste) polymers, Prog. Polym. Sci. 94 (2019) 1–32.
[8] H.L. Wang, Y. Yang, Y.Y. Liang, J.T. Robinson, Y.G. Li, A. Jackson, Y. Cui, H.J. Dai, Graphene-wrapped sulfur particles as a rechargeable Lithium–Sulfur battery cathode material with high capacity and cycling stability, Nano Lett. 11 (2011) 2644–2647.
[9] T.L. Kelly, T. Gao, M.J. Sailor, Carbon and Carbon/Silicon composites templated in rugate filters for the adsorption and detection of organic vapors, Adv. Mater. 23 (2011) 1776–1781.
[10] B.Z. Fang, J.H. Kim, M.S. Kim, J.S. Yu, Ordered hierarchical nanostructured carbon as a highly efficient cathode catalyst support in proton exchange membrane fuel cell, Chem. Mater. 21 (2009) 789–796.
[11] H.R. Abuzeid, A.F.M. EL-Mahdy, M.M.M. Ahmed, S.W. Kuo, Triazine-functionalized covalent benzoxazine framework for direct synthesis of N-doped microporous carbon, Polym. Chem. 10 (2019) 6010–6020.
[12] F. Zheng, Y. Yang, Q. Chen, High lithium anodic performance of highly nitrogen-doped porous carbon prepared from a metal-organic framework, Nat. Commun. 5 (2014) 5261–5270.
[13] W. Niu, L. Li, X. Liu, N. Wang, J. Liu, W. Zhou, Z. Tang, S. Chen, Mesoporous N-Doped carbons prepared with thermally removable nanoparticle templates: an efficient electrocatalyst for oxygen reduction reaction, J. Am. Chem. Soc. 137 (2015) 5555–5562.
[14] Y. Meng, D. Gu, F. Zhang, Y. Shi, H. Yang, Z. Li, C. Yu, B. Tu, D. Zhao, Ordered mesoporous polymers and homologous carbon frameworks: amphiphilic surfactant templating and direct transformation, Angew. Chem., Int. Ed. 44 (2005) 7053–7059.
[15] Z.Y. Wang, F. Li, N.S. Ergang, A. Stein, Effects of hierarchical architecture on electronic and mechanical properties of nanocast monolithic porous carbons and carbon − Carbon nanocomposites, Chem. Mater. 18 (2006) 5543–5553.
[16] M.G. Mohamed, A.F.M. El-Mahdy, M.M.M. Ahmed, S.W. Kuo, Direct synthesis of microporous bicarbazole-based covalent triazine frameworks for high-performance energy storage and carbon dioxide uptake, Chem.Plus.Chem. 84 (2019) 1767–1774.
[17] M.E. Casco, S. Kirchhoff, D. Leistenschneider, M. Rauche, E. Brunner, L. Borchardt, Mechanochemical synthesis of N-doped porous carbon at room temperature, Nanoscale 11 (2019) 4712–4718.
[18] X. Cui, Q. Yang, Y. Xiong, Z. Bao, H. Xing, S. Dai, Preparation of ordered N-doped mesoporous carbon materials via a polymer–ionic liquid assembly, Chem. Commun. 53 (2017) 4915–4918.
[19] P.X. Hou, H. Orikasa, T. Yamazaki, K. Matsuoka, A. Tomita, N. Setoyama, Y. Fukushima, T. Kyotani, Synthesis of nitrogen-containing microporous carbon with a highly ordered structure and effect of nitrogen doping on H_2O adsorption, Chem. Mater. 17 (2005) 5187–5193.
[20] J. Kou, L.B. Sun, Nitrogen-doped porous carbons derived from carbonization of a nitrogen-containing polymer: efficient adsorbents for selective CO_2 capture, Ind. Eng. Chem. Res. 55 (2016) 10916–10925.
[21] B. Kiskan, Y. Yagci, Thermally curable benzoxazine monomer with a photodimerizable coumarin group, J. Polym. Sci. Part A: Polym. Chem. 45 (2017) 1670–1676.
[22] K. Zhang, L.Han Han, P. Froimowicz, H. Ishida, A smart latent catalyst containing o-trifluoroacetamide functional benzoxazine: precursor for low temperature formation of very high Performance polybenzoxazole with low dielectric constant and high thermal stability, Macromolecules 50 (2017) 6552–6560.
[23] C. Wang, J. Sun, X. Liu, A. Sudo, T. Endo, Synthesis and copolymerization of fully bio-based benzoxazines from guaiacol, furfurylamine and stearylamine, Green Chem. 14 (2012) 2799–2806.
[24] M.G. Mohamed, S.W. Kuo, Functional silica and carbon nanocomposites based on polybenzoxazines, Macromol. Chem. Phys. 220 (2019) 1800306.
[25] M. Arslan, B. Kiskan, Y. Yagci, Benzoxazine-based thermoset with autonomous self-healing and shape recovery, Macromolecules 51 (2018) 10095–10103.
[26] K. Zhang, Y. Liu, H. Ishida, Polymerization of an AB-Type benzoxazine monomer toward different polybenzoxazine networks: when diels–alder reaction meets benzoxazine chemistry in a single-component resin, Macromolecules 52 (2019) 7386–7395.
[27] A.F.M. El-Mahdy, S.W. Kuo, Direct synthesis of poly(benzoxazine imide) from an ortho-benzoxazine: its thermal conversion to highly cross-linked polybenzoxazole and blending with poly(4-vinylphenol), Polym. Chem. 9 (2018) 1815–1826.
[28] W.H. Hu, K.W. Huang, S.W. Kuo, Heteronucleobase functionalized benzoxazine: synthesis, thermal properties, and self assembled structure formed through multiple hydrogen bonding interactions, Polym. Chem. 3 (2012) 31546–31554.
[29] S.W. Kuo, Y.C. Wu, C.F. Wang, K.U. Jeong, Preparation low surface energy polymer materials by minimizing intermolecular hydrogen bonding interaction, J. Phys. Chem. C. 113 (2009) 20666–20673.
[30] M.G. Mohamed, R.C. Lin, K.C. Hsu, W. Zhang, X. Zhong, S.W. Kuo, Mediated surface properties of polybenzoxazines, in: H. Ishida, P. Froimowicz (Eds.), Advanced and Emerging Polybenzoxazine Science and Technology, Elsevier, Amsterdam, 2017, pp. 205–219.
[31] M.G. Mohamed, K.C. Hsu, S.W. Kuo, Bifunctional polybenzoxazine nanocomposites containing photo-crosslinkable coumarin units and pyrene units capable of dispersing single-walled carbon nanotubes, Polym. Chem. 6 (2015) 2423–2433.
[32] M.G. Mohamed, R.C. Lin, S.W. Kuo, Polybenzoxazine/carbon nanotube composites, in: H. Ishida, P. Froimowicz (Eds.), In Advanced and Emerging Polybenzoxazine Science and Technology, Elsevier, Amsterdam, 2017, pp. 725–738.
[33] S. Zhang, Q. Ran, Q. Fu, Y. Gu, Thermal responsiveness of hydrogen bonding and dielectric property of polybenzoxazines with different Mannich bridge structures, Polymer 175 (2019) 302–309.
[34] C.C. Yang, Y.C. Lin, P.I. Wang, D.J. Liaw, S.W. Kuo, Polybenzoxazine/single-walled carbon nanotube nanocomposites stabilized through noncovalent bonding interactions, Polymer 55 (2014) 2044–2050.
[35] M.G. Mohamed, C.H. Hsiao, F. Luo, L. Dai, S.W. Kuo, Multifunctional polybenzoxazine nanocomposites containing photoresponsive azobenzene units, catalytic carboxylic acid groups, and pyrene units capable of dispersing carbon nanotubes, RSC Adv. 5 (2015) 45201–45212.
[36] C.R. Araz, H. Ishida, F.H. Maurer, Quantifying dispersion in graphene Oxide/Reactive benzoxazine monomer nanocomposites, Macromolecules 47 (2014) 3685–3692.
[37] H.K. Shih, C.C. Hsieh, M.G. Mohamed, C.Y. Zhu, S.W. Kuo, Ternary polybenzoxazine/POSS/SWCNT hybrid nanocomposites stabilized through supramolecular interactions, Soft Matt. 12 (2016) 1847–1856.
[38] S.W. Kuo, F.C. Chang, POSS related polymer nanocomposites, Prog. Polym. Sci. 36 (2011) 1649–1696.
[39] W.C. Chen, S.W. Kuo, Ortho-imide and allyl groups effect on highly thermally stable Polybenzoxazine/Double-Decker-Shaped polyhedral silsesquioxane hybrids, Macromolecules 51 (2018) 9602–9612.
[40] H.K. Fu, C.F. Huang, S.W. Kuo, H.C. Lin, D.R. Yei, F.C. Chang, Effect of an organically modified nanoclay on low-surface-Energy materials of polybenzoxazine, Macromol. Rapid Commun. 29 (2008) 1216–1220.
[41] Y.C. Ye, Y.J. Huang, F.C. Chang, Z.G. Xue, X.L. Xie, Synthesis and characterization of thermally cured polytriazole polymers incorporating main or side chain benzoxazine crosslinking moieties, Polym. Chem. 5 (2014) 2863–2871.
[42] N. Liu, L. Li, L. Wang, S. Zhang, Organic-inorganic polybenzoxazine copolymers with double decker silsesquioxanes in the main chains: synthesis and thermally activated ring-opening polymerization behavior, Polymer 109 (2017) 254–265.
[43] G.P. Hao, W.C. Li, D. Qian, G.H. Wang, W.P. Zhang, T. Zhang, A.Q. Wang, F. Schuth, H.J. Bongard, A.H. Lu, Structurally designed synthesis of mechanically stable poly (benzoxazine-co-resol)-Based porous carbon monoliths and their application as high-performance CO_2 capture sorbents, J. Am. Chem. Soc. 133 (2011) 11378–11388.
[44] L. Wan, J. Wang, Y. Sun, C. Feng, K. Li, Polybenzoxazine-based nitrogen-containing porous carbons for high-performance supercapacitor electrodes and carbon dioxide capture, RSC Adv. 5 (2015) 5331–5342.
[45] J.Y. Wu, M.G. Mohamed, S.W. Kuo, Directly synthesized nitrogen-doped microporous carbons from polybenzoxazine resins for carbon dioxide capture, Polym. Chem. 8 (2017) 5481–5489.
[46] R.C. Lin, M.G. Mohamed, K.C. Hsu, J.Y. Wu, Y.R. Jheng, S.W. Kuo, Multivalent photo-crosslinkable coumarin containing polybenzoxazines exhibiting enhanced thermal and hydrophobic surface properties, RSC Adv. 6 (2016) 10683–10696.
[47] R. Wei, Y. He, X. Wang, Diblock copolymers composed of a liquid crystalline azo block and a poly(dimethylsiloxane) block: synthesis, morphology and photo-responsive properties, RSC Adv. 4 (2014) 58386–58396.
[48] M.G. Mohamed, C.H. Hsiao, F. Luo, L. Dai, S.W. Kuo, Multifunctional polybenzoxazine nanocomposites containing photoresponsive azobenzene units, catalytic carboxylic acid groups, and pyrene units capable of dispersing carbon nanotubes, RSC Adv. 5 (2015) 45201–45212.
[49] M.G. Mohamed, W.C. Su, Y.C. Lin, C.F. Wang, J.K. Chen, K.U. Jeong, S.W. Kuo, Azopyridine-functionalized benzoxazine with $Zn(ClO4)_2$ form high-performance polybenzoxazine stabilized through metal–ligand coordination, RSC Adv. 4 (2014) 50373–50385.
[50] Q.L. Zhao, X.Y. Wang, C. Wu, J. Liu, H. Wang, J. Gao, Y.W. Zhang, H.B. Shu, Supercapacitive performance of hierarchical porous carbon microspheres prepared by simple one-pot method, J. Power Sources 254 (2014) 10–17.
[51] Y. Liu, L. Cao, J. Luo, Y. Peng, Q. Ji, J. Dai, J. Zhu, X. Liu, Biobased nitrogen- and oxygen-codoped carbon materials for high-performance supercapacitor, ACS Sustainable Chem. Eng. 7 (2019) 2763–2773.
[52] W. Shi, X. Zhang, Y. Ji, Z. Zhao, W. Li, X. Jia, Sustainable preparation of bio-based polybenzoxazine resins from amino acid and their application in CO_2 adsorption, ACS Sustainable Chem. Eng. 7 (2019) 17313–17324.
[53] B. Adeniran, R. Mokaya, Is N-Doping in porous carbons beneficial for CO_2 storage? Experimental demonstration of the relative effects of pore size and N-Doping, Chem. Mater. 28 (2016) 994–1001.
[54] G.P. Hao, W.C. Li, D. Qian, A.H. Lu, Rapid synthesis of nitrogen-doped porous carbon monolith for CO_2 capture, Adv. Mater. 22 (2010) 853–857.